Available online at www.sciencedirect.com
ScienceDirect
Ceramics International 34 (2008) 157–164
CERAMICS INTERNATIONAL
www.elsevier.com/locate/ceramint

Ferroelectric lithography

Dongbo Li *, Dawn A. Bonnell

Department of Materials Science and Engineering, University of Pennsylvania, Philadelphia, PA 19104, USA

Received 1 August 2006; received in revised form 7 August 2006; accepted 20 September 2006
Available online 4 December 2006

Abstract

The fact that domain polarization affects the surface properties suggests a method to direct chemical reactions on ferroelectric substrates. In combination with domain manipulation at small scales, a new lithography process is developed to assemble several classes of nanostructures. Three domain patterning techniques, which employ contact electrodes, SPM and e-beam are introduced, with focus on the physical interactions between electrons and ferroelectrics. The effects of electron beam parameters on polarization reorientation are quantified and it is shown that both positive and negative polarization can be achieved depending on conditions. Potential applications of ferroelectric lithography on fabrication of complex structures are illustrated.
Published by Elsevier Ltd and Techna Group S.r.l.

Keywords: Ferroelectric; Patterning; Lithography; Nanostructure

1. Introduction

Ferroelectric compounds have attracted increasing interest in recent years due to their applications on the nonvolatile ferroelectric random access memories (NVFRAMs) [1,2]. In the last decade, the advance in thin film processing motivates intensive studies on this class of materials at the nanometer length scale. The development of scanning probe tools facilities these studies, leading to better understanding of ferroelectric behavior at this scale. Of particular importance to this field is piezoresponse force microscopy [3] and transport related scanning probes [4]. Application of SPM has rendered some significant achievements in this field, including manipulation of domains as small as 20 nm in diameter [5], visualization of the polarization decay at the sub-grain level [6], and direct observation of domain nucleation and growth during polarization reversal [7].

In the studies of sub-micrometer sized ferroelectric devices, most research is conducted on details of interface charge, residual stress, and mechanical constraint in order to achieve the best performance. The nanometer scaled SPM characterization in combination with theoretical concepts has enabled researchers to address mechanisms of domain switching, origins of imprint, and fatigue [8–11]. These studies have led to insights regarding the effect of local electrostatic fields and strain at interfaces on domain switching and stability.

Despite the significant progress in development of ferroelectric thin films and devices, less attention has been focused on ferroelectric surface properties over the last few years. A new field was developed recently based on the fact that ferroelectric polarization affects the surface properties, which can be exploited to control surface reactions. Ferroelectric surfaces facilitate a new lithography process for complex structure fabrication [12,13]. Ferroelectric lithography combines the domain patterning at submicron meter scale with domain specific chemical reactions to assemble multi-components (metal nanoparticles, organic molecules, peptides, tubes, wires, etc.) into complex structures. This paper will describe the effect of polarization on surface properties in model ferroelectric compound and illustrate three approaches to polarization patterning. The domain specific reactivity and patterning will then be combined into a fabrication process that is demonstrated on several classes of nanostructures.

2. Surface properties of ferroelectrics

Domain polarization has a large effect on the surface properties of ferroelectric oxides, giving rise to some domain

* Corresponding author.
E-mail addresses: dongboli@seas.upenn.edu (D. Li), bonnell@lrsm.upenn.edu (D.A. Bonnell).

0272-8842/$32.00. Published by Elsevier Ltd and Techna Group S.r.l.
doi:10.1016/j.ceramint.2006.09.021

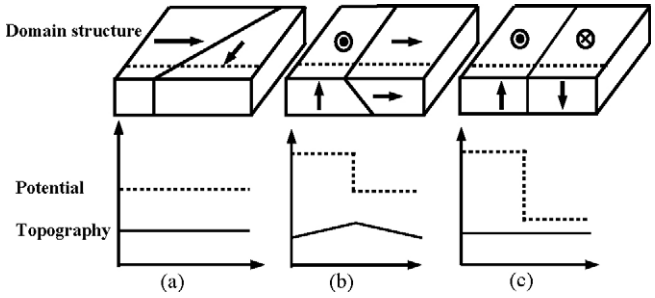

Fig. 1. Possible domain orientations intersecting a (1 0 0) surface of tetragonal $BaTiO_3$. Arrows represent the orientations of polarization vectors. (a) 90° *a*1–*a*2 boundary, (b) 90° c^+–*a*1 boundary, and (c) 180° c^+–c^- boundary. Shown below are the surface potentials (dot) and topographies (solid) expected along the dotted lines.

specific phenomena, which attract much attention in this field. From an energetic consideration, spontaneous polarization is screened at the surface either by free charges inside the crystal or by external media, such as adsorption of ions or charged particles. Consequently, the termination of domains at a surface results in a large surface charge, the magnitude of which depends on the orientation of the polarization vector. This is illustrated in Fig. 1 for a model system $BaTiO_3$ (1 0 0), which is a tetragonal perovskite that contains domains oriented along [1 0 0] directions, and therefore oriented 90° or 180° with respect to each other. Surface domains are easily imaged by scanning surface potential microscopy (Kelvin force microscopy) and by piezoresponse force microscopy [14,15]. Fig. 2 illustrates typical surface domain patterns on single crystal $BaTiO_3$ (1 0 0) surface. Note that the difference in surface charge between *a*- and *c*-domains is of a different magnitude than that between c^+ and c^- domains and that an *a*–*c* domain has a physical surface corrugation due to lattice parameter differences in these directions.

Kalinin and Bonnell [16,17] studied the effect of the ferroelectric-to-paraelectric phase transition on surface charge, and found that the charge exhibited different dynamics than did the structural phase transition. The situation is schematically illustrated in Fig. 3. Quantification the observation of domain structure during phase transition addresses some important understanding on ferroelectric surface. Spontaneous polarization is partially or completely screened by surface charges so that surface potential microscopy measures the compensating effect. Therefore, under ambient conditions, the sign of surface charges in surface potential measurement is opposite to that of polarization charges. Of the most importance for the present discussion, there is a separation of charge carriers depending on the sign of the domain. Positive charges or oriented dipoles compensate negative domains and vice versa. This suggests that domain polarization can have a significant effect on local surface interactions.

Two types of polarization-dependent surface effects can occur on ferroelectric domains. The first one is based on the electrostatic attraction of surface charge, which results in adsorption of oppositely charged media. This case was demonstrated in the 1950s in the decoration of ferroelectric domains using sulfur and lead oxide [18]. The second class of surface interaction relies on the fact that surface charges affect the electronic structure at ferroelectric oxides surface. Depending on the sign of polarization, surface charge raises or lowers the energies of orbitals in the vicinity of surface, resulting in near surface band bending and formation of space charge region. From this point of view, it is clear that surface reactions involving electron or hole donations will selectively occur on some polarization specific regions at substantially high rates.

In order to excite this class of domain specific reaction, an extrinsic source of carriers, such as photo-generated electron–hole pairs, is required. Since ferroelectric oxides are intrinsically semiconductors with band gaps ranging from 3 to 4.5 eV, irradiation with super band-gap radiation can result in the formation of electron–hole pairs that can accumulate to the appropriate domain regions. A direct observation of this effect is illustrated in Fig. 4, which shows *in situ* measurement of surface charge in the presence and absence of UV illumination of $BaTiO_3$ (1 0 0). These results show that photo-generated carriers can be separated and moved to appropriate domain regions for participation in domain specific surface reactions.

3. Patterning ferroelectric polarization at surfaces

As the basis of the capacitor and nonvolatile storage industries, it has been long known that ferroelectric domains can be switched with electrodes. In the last several years, development of high density of memory devices requires domain polarization manipulation at surface in the micrometer

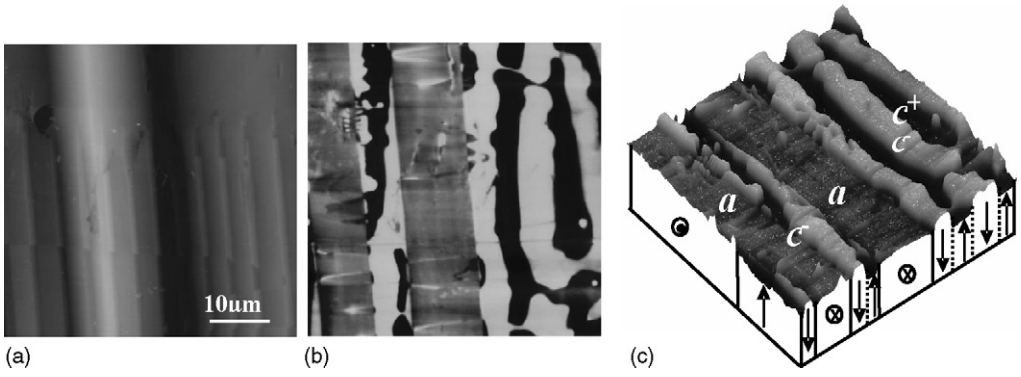

Fig. 2. Surface topography (a), surface potential (b), and schematics of domain structures (c) in an *a*-domain region with *c*-domain wedges.

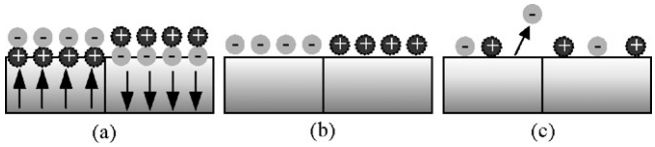

Fig. 3. Schematic diagram of the surface charge compensation processes showing polarization charge terminating at the arrows and compensation charge. Below the Curie temperature (a), immediately after transition (b), and some time after phase transition (c).

or even nanometer scale. We will introduce three mechanisms for surface polarization patterning here: microcontact electrodes, scanning probe tips, and electron beam induced charging.

3.1. Contact electrode patterning

The fact that micro-printing can produce small patterns with high throughput and amenability to scaleable processing provides the unique opportunity to pattern domains by micron contact electrode. The process is illustrated in Fig. 5(a). The polymer stamps with desired patterns are fabricated using traditional printing techniques, such as e-beam lithography, which is appropriate for the micrometer length scale. Metals will then be coated on the stamps to produce the patterned electrodes. An electric field is applied through this patterned electrode to the surface of a ferroelectric substrate, giving rise to a domain polarization manipulation. Switching mechanism is the same with domain reorientation with traditional parallel electrodes, which involving the heterogeneous domain nucleation at the interface followed by domain growth. The pattern in Fig. 5(b) is not particularly small, but demonstrates the effectiveness of the stamp electrode in switching.

3.2. Scanning probe patterning

The second approach to surface polarization patterning is to extend the concept of a contact electrode to a scanning probe tip, which is illustrated in Fig. 6(a). In this method, a DC voltage is applied to the SPM tip when scanning over the ferroelectric surface. A local electric filed induced with the tip can switch domain polarization at surface, when its intensity is sufficiently high. The switching mechanism also involves the domain nucleation followed by forward growth and sidewise expansion processes, but the geometry of the field differs from that of a planar top electrode. Due to the small size of the tip radius, the ultimate limit of domain patterning will be limited by the crystalline structure of the substrate. Soon after the development of scanning probe techniques, many studies have been conducted on controlling ferroelectric polarization by SPM tip, with the particular interests in determining the minimum size of a stable domain and investigating domain wall dynamics. Domains in the sub-100 nm size range were produced in several studies [19]. A typical pattern is illustrated in Fig. 6(b) for 150 nm PZT thin films with a 10 nm underlying Pt electrode.

3.3. Electron beam patterning

The third approach to domain patterning is based on the interaction of injected electrons with a ferroelectric surface.

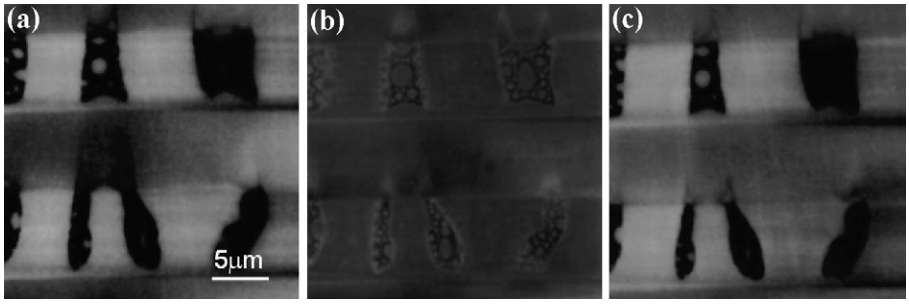

Fig. 4. Scanning surface potential microscopy of $BaTiO_3$ (1 0 0) before (a), during (b), and after (c) illumination with UV light. Optically generated carriers selectively accumulate at positive or negative domains and compensate the polarization charge.

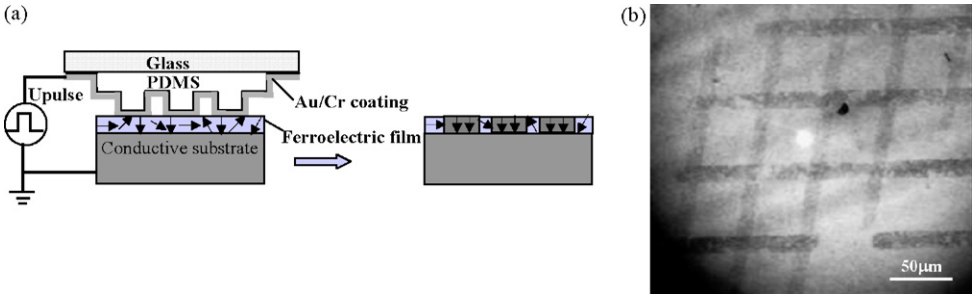

Fig. 5. Schematic of microcontact electrode ferroelectric domain patterning (a), and an optical micrograph of pattern on a PZT thin film generated by microcontact electrode (b).

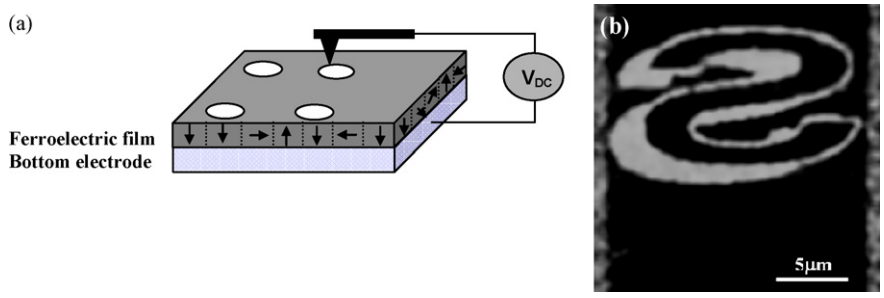

Fig. 6. Schematic of direct poling domains in ferroelectric thin film using AFM tip (a), and a PFM phase image (b) of a complex pattern written by AFM tip.

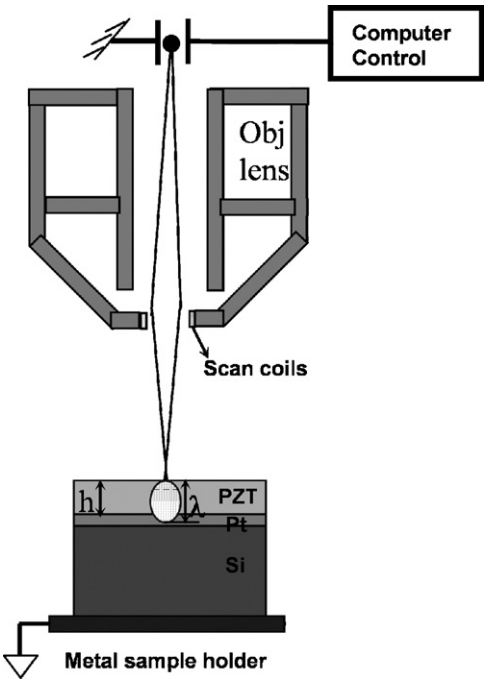

Fig. 7. Experimental setup for electron beam ferroelectric lithography and surface charge measurement. A scanning electron microscope equipped with lithography software is used to expose the sample to a focused electron beam. Electrons penetrate the sample to a depth (λ) and develop charge on surface.

Macroscopic features were produced by e-beam irradiation on single crystal $LiNbO_3$ [20,21] in the early 1990s. Nanometer sized domain patterns by e-beam writing and quantitative aspects of the poling mechanism have been demonstrated on polycrystalline PZT thin films in the recent studies [22,23].

Fig. 7 schematically shows the experimental setup. Under electron irradiation, elastic and inelastic collisions in the crystal lead to the excitation of secondary electrons and backscattering of incident electrons from an insulator surface. Secondary electrons sufficiently close to the surface (less than 50 nm) are emitted from the surface, while the other electrons are either trapped in defect sites or self-trapped as polarons in the crystal. In most of the cases the number of incident electrons is not equal to that of the emitted electrons, which causes surface charge. Domain reorientation near the surface could occur when the field generated by the surface charge is stronger than the coercive field of the ferroelectric compound. Polarization will be reoriented with a negative domain termination near the surface by positive net surface charge. On the other hand, positive domain reorientation happens for negative surface charge.

Fig. 8 shows the dosage dependence of polarization reorientation. The switching ratio is determined by the *c*-orientation area over the total irradiated area. A threshold dosage exists for the onset of polarization switching, which is around 500 μC/cm^2. Below this value no effect is observed. At dosages higher than 1500 μC/cm^2, around 90% of the domains are reoriented and this is the saturated percentage. The number of switched domains increases monotonically between these two values. Since the orientation distributes randomly in the original polycrystalline film, the domains with the most favorable orientation switch at first when the local electrical field reaches the lower critical value. With increasing electrical field, some other domains could be further switched until all the possible domains have been switched.

Since the cross-sections for excitations causing electron emission are relatively large, positive charge could be easily

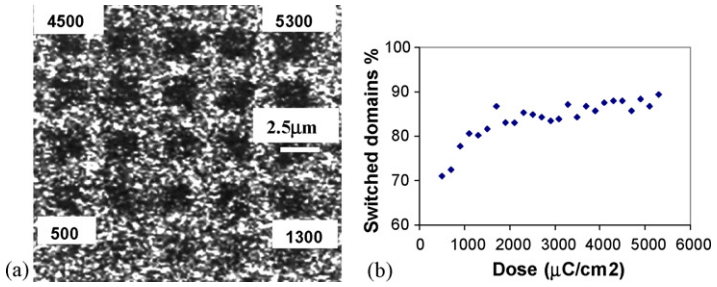

Fig. 8. (a) PFM phase image (over 20 μm × 20 μm area) showing negative domain polarization switched by electron beam of 10 keV, 30 pA, and dosages ranging from ∼500 to 5000 μC/cm^2. The exposure is increased from left to right and from bottom to top in the figure with the dosage values (in μC/cm^2) indicated for the corner positions. The darker regions are the negatively polarized domains. (b) The fraction of c^- domains increases with electron dosage.

developed on an insulator surface. However, negative charge development is less straightforward. With constant electron beam energy, the dosage is related to the amount of charge accumulated on the surface. In an insulating thin film under electron irradiation, the surface potential is [24,25]:

$$V_S = \frac{Q_T}{\pi\varepsilon_0(1+\varepsilon_r)a} f \quad (1)$$

where Q_T is the total trapped charge, ε_r is the relative permittivity of the material, a is the spot diameter of electron beam, and f is a complex factor between 0 and 1 that accounts for the geometry of the thin film [26]. If electron trapping in the PZT film is due to intrinsic defects with a reasonable density of 10^{20} cm^{-3} [27], the resulting surface potential is 51 mV, resulting in a field less than the coercive field (~30–100 kV/cm) of PZT. Since the domains do switch under the surface charge filed, the electrons must be trapped by some additional mechanisms. One possibility is that e-beam irradiation induces further defects which could accommodate more charges and intensify the internal electrical field inside the film.

Fig. 9 shows the beam current dependence of domain reorientation. With beam current <0.05 nA, local electric field is always pointing perpendicularly into the film with different beam energy and domains reorient with c^- termination. With current >1 nA, electric field is reversed and domains reorient with c^+ termination. At intermediate currents, the sign of local electric field depends on the beam energy. The surface charge and resulting electric field is influenced by the beam current through the electron emission yield, which is the intensity ratio of emitted electrons including secondary (I_S), backscattered (I_B), and leakage electrons (I_L), to primary electrons (I_0):

$$\sigma = \frac{I_B + I_S + I_L}{I_0} \quad (2)$$

For thin film geometry an important factor is the electron penetration depth [28]:

$$\lambda = \frac{0.0276AE^{1.67}}{Z^{0.89}d} \quad (3)$$

where A is the atomic weight in g/mol, E is the electron beam energy in keV, Z is the average atomic number, and d is the density in g/cm^3 (A = 235 g/mol, Z = 63, and d = 7.5 g/cm^3 for PZT). When film thickness h is smaller than λ, some electrons will leak through the Pt film and the silicon substrate (see Fig. 7). Substantial numbers of electrons enter the underlying Pt/Si substrate at the beam energy above ~10 keV. The excitation cross-sections that result in electron emission at the surface (I_B and I_S) also scale with the beam energy. As beam energy increases, more electrons are lost at the surface and the PZT bulk should contain less negative charge. These two opposite effects determine the internal electrical field.

The electron yield typically exhibits the behavior that is schematically superimposed on Fig. 9 for insulating materials. σ increases at lower beam energy due to the increasing excitation cross-section with beam energy. However, σ decreases at higher beam energy due to the reducing number of electrons trapped within the film. σ maximizes at certain beam energy with the combination of these two effects for a given beam current. At low current density (10^6 pA/cm^2), polarization is always reoriented negatively, implying a positive surface charge. At high current density (10^9 pA/cm^2), the same beam dosage and beam energy yield positively switched polarization.

In summary, both positively and negatively poled features can be created under various e-beam irradiation conditions. This method provides the opportunity for nanometer domain engineering due to the length scale accessible to conventional e-beam tools.

4. Domain specific reactivity at ferroelectric surfaces

The combination of the ability to pattern templates of ferroelectric domains and the fact that domain orientation mediates surface interactions leads to an approach for sophisticated surface chemical control. Photoreaction is a simple and illustrative example of the generality of the concept.

Giocondi and Rohrer have demonstrated that domain polarization overwhelms any other crystal structural factors and dominates the photochemical properties of ferroelectric

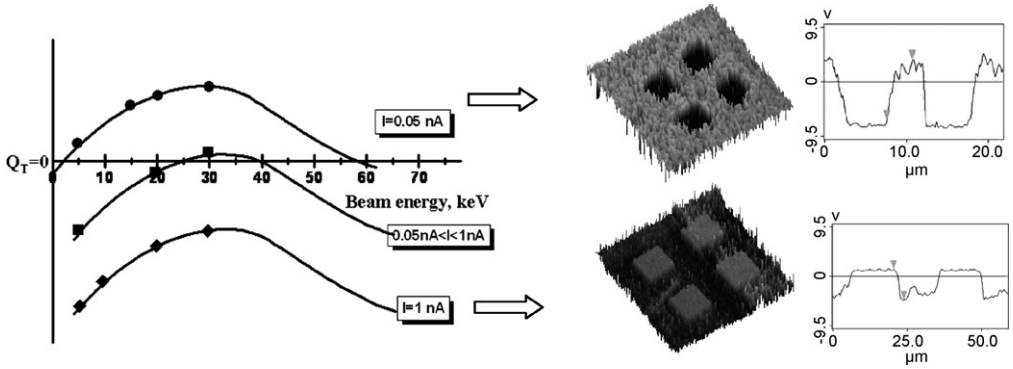

Fig. 9. Polarization reorientation dependence on beam energy and current. Dots represent experimental determination of domain polarity superimposed on a schematic representation of Q_T, which should follow the expected trend of the total electron emission yield σ for an insulator. The intercept along the y-axis represents Q_T = 0, which corresponds to σ equal to 1. PFM phase images (middle) and cross-section analysis (right) showing (bottom) positive polarization from a 1 nA beam and (top) negative polarization from a 0.05 nA beam, switched with electron beam of 3000 μC/cm^2 and 30 keV.

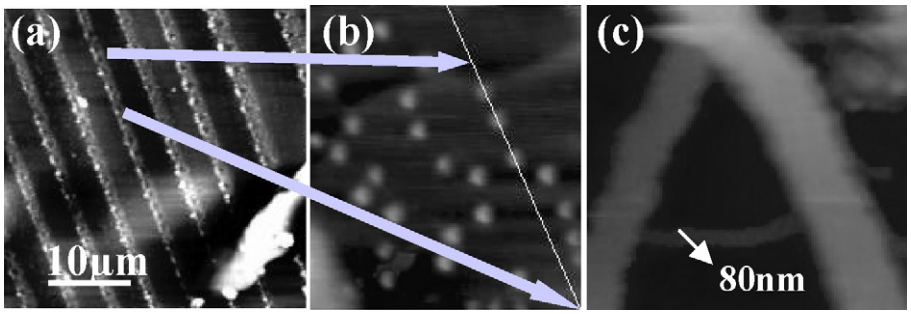

Fig. 10. Topographic images of Ag particles deposited on PZT surface by ferroelectric nanolithography. Depending on reaction conditions 3-D structures of multiple vertical layers of particles (a) or isolated 3 nm particles (b), and submicron sized rod (c) can be produced.

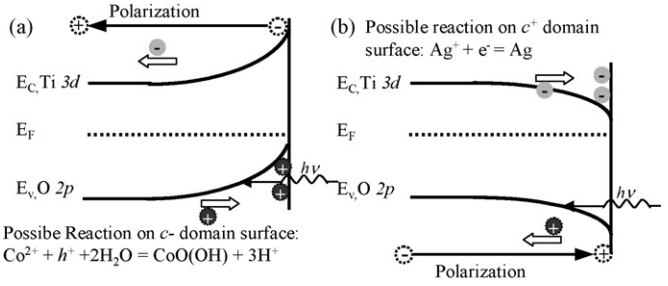

Fig. 11. Schematic diagram of band bending in the ferroelectric perovskite crystals in the c^- (a) and c^+ (b) domain regions. For $BaTiO_3$ and $PbTiO_3$ E_v is the top of the band associated with oxygen 2p orbitals and E_c is the bottom of the band associated with the titanium 3d orbitals.

semiconductors [29–31]. To obtain complex assemblies, Kalinin et al. [12,32] proposed a directed process, ferroelectric nanolithography, which can position multiple components into predefined configurations. Desired domain patterns are firstly achieved on ferroelectric substrates using any of the methods outlined above. Subsequently, photochemical reactions are confined on the appropriate domain surface regions by placing the patterned substrate into an aqueous metal salt solution with the irradiation of super band gap UV light. By controlling the reaction conditions it is possible to produce patterns with 3–10 nm particles in 1-D arrays or build 3-D structures with multiple layers of nanoparticles. Fig. 10 shows Ag nanoparticles deposited on a patterned PZT thin film.

As noted above, the reaction mechanism is based on electron exchange at the surface. Fig. 11 illustrates the energies associated with the process and typical oxidation and reduction reactions. For the case of titanates, the bottom of the conduction band is predominantly formed by Ti 3d orbitals, while the top of the valence band has predominantly O 2p character. In the negative domain region (c^-), surface charge is positive, causing the upward band bending and accumulation of holes at the surface. In the positive domain region (c^+), surface charge is negative associated with downward band bending and formation of electron region. As the result, surface reactions involving electron or holes donations will selectively occur at specific domain regions. Surface reactions involving electron donation will occur at substantially higher rates at c^+ domains than at c^- domains, while a reaction based on holes donation will occur over the negatively poled domains [32].

Except for inert metals (Ag, Au, Pt, Rh, and Pd) deposition, multi-elements photodeposition, and some transition metals photodeposition have been achieved, which are shown in Fig. 12(a–d). Fig. 12(a) shows a region on which Ag and Au nanoparticles co-deposited on c^+ domains from a solution with Ag and Au ions. To extend this approach to a broader material set, reactions for magnetic Ni-, Fe-, and Co-based particles were developed, with the deposition results shown in Fig. 12(b–d), respectively. Noted that Fe- and Ni-based particles are deposited on c^+ domain regions, while Co-based particles are on c^- domain regions. Fig. 12(d) shows a pattern

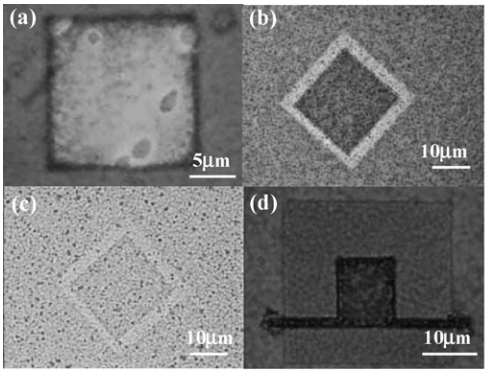

Deposition	Products
Inert metals	Ag, Au, Pt, Rh and Pd
Magnetic metals	Fe-, Co-, Ni-based compounds
Multi-metals co-deposition	Ag+Au
Multi-metals sequent deposition	Ag-Au, Ag-Co

Fig. 12. Optical micrographs of nanoparticles photo-reacted on patterned PZT substrates. (a) Au and Ag simultaneously deposited on c^+ domains, (b) Ni-based and (c) Fe-based particles on c^+ domains. (d) Co-based particles on c^- domains followed by Ag on c^+ domains. Inset table on the right shows the summary of photoreactions and resulting products.

in which gold nanoparticles surround cobalt oxide nanoparticles, which are sequentially deposit on the appropriate domains since the cobalt and gold nanoparticles undergo opposite electron exchange reactions. From the position of resulting products, it can be inferred that surface interactions involving electrons occur in the Fe- and Ni-depositions. On the contrary, reactions involving holes occur in the Co-deposition. Therefore, the possible surface reactions in Fe-, Ni-, and Co-depositions are:

$$Fe^{2+} + 2e^- \rightarrow Fe$$

$$Ni^{2+} + 2e^- \rightarrow Ni$$

$$Co^{2+} + h^+ \rightarrow CoO(OH) + 3H^+$$

Due to the multiple valences, magnetic metal photoreactions are more complicated than inert metal deposition. On the one hand, magnetic metal deposition can involve several possible chemical reactions. Taking iron as an example, the possible reactions are listed as follows:

1. $2Fe^{2+} + 2h^+ + 3H_2O \rightarrow Fe_2O_3 + 6H^+$
2. $3Fe^{2+} + 2h^+ + 4H_2O \rightarrow Fe_3O_4 + 8H^+$
3. $Fe^{2+} + 2e^- \rightarrow Fe$
4. $Fe + O_2 \rightarrow Fe_2O_3$
5. $Fe_2O_3 + O_2 \rightarrow Fe_3O_4$

Whether photo-oxidization or photo-reduction occurs can only be determined by the position of the resulting product. On the other hand, in an aqueous environment, the surface of the deposited particles is more likely to be oxidized, and therefore, the final composition of the particles cannot be decided without further characterization. Magnetic Force Microscopy has verified the magnetic properties of the Fe-, Co-, and Ni-based nanoparticles.

5. Assembling multi-component structures

In combination with some special chemical reactions, ferroelectric nanolithography allows multiple nanostructures of diverse materials to be positioned in predefined locations. This is illustrated in Fig. 13. Detailed procedures consist of pattering domains on a ferroelectric substrate, confining surface reactions on domain specific regions, and assembling multi-components into predefined configurations. It has been demonstrated that thiolated alkanes react only with Ag and Au particles, which are photodeposited on patterned ferroelectric thin film, and not with the oxide substrate [33]. This method can be easily extended to attach more organic molecules with some special functionality, such as electrical or optical properties, on ferroelectric surface to form some complex nanostructure. Several factors emphasize how general this process can be.

- A wide library of ferroelectric substrates, including single crystal, polycrystalline or epitaxial thin film, and ferroelectric polymer.
- A variety of electron exchange reactions.
- Attachment of much more various organic molecules.
- The possibility to fabricate nano based devices and then be integrated into large systems simultaneously.
- Assembly of any nanostructures (nanotubes, nanowire, optical quantum dots, etc.) with appropriate end-groups.

In summary, ferroelectric nanolithography has the ability to assembly multiple types of nanostructures into predefined locations and offers the potential to produce nanostructured devices for new families of applications.

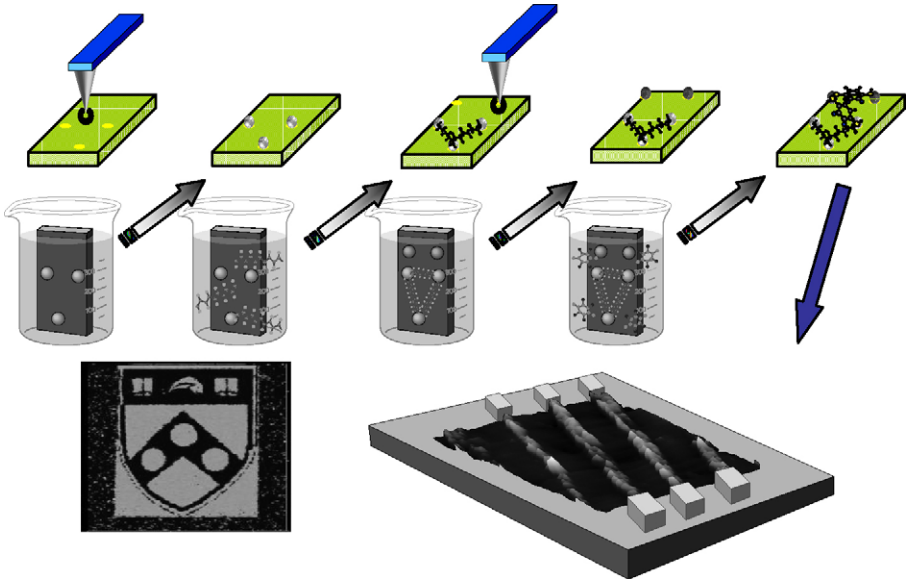

Fig. 13. Schematic diagram of ferroelectric lithography for directed assembly of multiple component structures in predefined locations. Sequential steps include: pattern polarization orientation, site selective reaction of component 1 (metal), chemically selective reaction of component 2 (organic molecule), new polarization pattern, selective reaction of component 3, etc. The lower right image shows 3 nm particles in a linear array. Polarization patterning is illustrated in the lower left which shows polarization vectors perpendicular to the surface in a PFM image.

6. Conclusions

Spontaneous polarization of ferroelectric materials significantly affects the local surface properties, which is examined in model single crystal system. Based on the domain controlling by contact electrode, scanning probe and electron beam, and sequent domain specific reactions, ferroelectric lithography is developed to fabricate complex nanostructures. This technique provides the opportunity to produce multi-components configurations on ferroelectric substrate.

References

[1] R. Ramesh, Thin Film Ferroelectric Materials and Devices, Kluwer Academic Publishers, Boston/Dordrecht/London, 1997.
[2] J.F. Scott, C.A. Paz de Araujo, Science 246 (1989) 1400.
[3] A. Gruverman, O. Auciello, H. Tokumoto, J. Vac. Sci. Technol. B 14 (1996) 602.
[4] D.A. Bonnell, R. Shao, Curr. Opin. Solid State Mater. Sci. 7 (2003) 161.
[5] A. Gruverman, O. Auciello, H. Tokumoto, Annu. Rev. Mater. Sci. 28 (1998) 101.
[6] A. Gruverman, H. Tokumoto, S.A. Prakash, S. Aggarwal, B. Yang, M. Wutting, R. Ramesh, O. Auciello, V. Venkatesan, Appl. Phys. Lett. 71 (1997) 3492.
[7] S. Hong, E.L. Colla, E. Kim, D.V. Taylor, A.K. Tagantsev, P. Muralt, K. No, N. Setter, J. Appl. Phys. 86 (1999) 607.
[8] C.S. Ganpule, V. Nagarajan, S.B. Ogale, A.L. Roytburd, E.D. Williams, R. Ramesh, Appl. Phys. Lett. 77 (2000) 3275.
[9] A. Gruverman, B.J. Rodriguez, A.I. Kingon, R.J. Nemanich, A.K. Tagantsev, J.S. Cross, M. Tsukada, Appl. Phys. Lett. 83 (2003) 728.
[10] E.L. Colla, S. Hong, D.V. Taylor, A.K. Tagantsev, N. Setter, Appl. Phys. Lett. 72 (1998) 2763.
[11] M. Grossmann, O. Lohse, D. Bolten, U. Boettger, R. Waser, J. Appl. Phys. 92 (2002) 2688;
M. Grossmann, O. Lohse, D. Bolten, U. Boettger, T. Schneller, R. Waser, J. Appl. Phys. 92 (2002) 2680;
P. Gerber, C. Kügeler, U. Ellerkmann, P. Schorn, U. Böttger, R. Waser, Appl. Phys. Lett. 86 (2005) 112908.
[12] S.V. Kalinin, D.A. Bonnell, T. Alvarez, X. Lei, Z. Hu, R. Shao, J.H. Ferris, Adv. Mater. 16 (2004) 795.
[13] S.V. Kalinin, D.A. Bonnell, T. Alvarez, X. Lei, Z. Hu, J. Ferris, Q. Zhang, S. Dunn, Nano Letters 2 (2002) 589.
[14] R. Lüthi, H. Haefke, K.-P. Meyer, L. Howald, H.-J. Güntherodt, J. Appl. Phys. 74 (1993) 7461.
[15] A. Gruverman, O. Kolosov, J. Hatano, K. Takahashi, H. Tokumoto, J. Vac. Sci. Technol. B 13 (1995) 1095.
[16] S.V. Kalinin, D.A. Bonnell, J. Appl. Phys. 87 (2000) 3950.
[17] S.V. Kalinin, D.A. Bonnell, Appl. Phys. Lett. 78 (2001) 1116.
[18] G.L. Pearson, W.L. Feldmann, J. Phys. Chem. Solids 9 (1958) 28.
[19] T. Tybell, C.H. Ahn, J.-M. Triscone, Appl. Phys. Lett. 72 (1998) 1454;
L.M. Eng, M. Bammerlin, C. Loppacher, M. Guggisberg, R. Bennewitz, R. Luthi, E. Meyer, T. Huser, H. Heinzelmann, H.J. Guntherodt, Ferroelectrics 222 (1999) 411.
[20] M. Yamada, K. Kishima, Electron. Lett. 27 (1991) 828.
[21] J. He, S.H. Tang, Y.Q. Qin, P. Dong, H.Z. Zhang, C.H. Kang, W.X. Sun, Z.X. Shen, J. Appl. Phys. 93 (2003) 9943.
[22] J.H. Ferris, D.B. Li, S.V. Kalinin, D.A. Bonnell, Appl. Phys. Lett. 84 (2004) 774.
[23] D.B. Li, D.R. Strachan, J.H. Ferris, D.A. Bonnell, J. Mater. Res. 21 (2006) 935.
[24] T. Thome, D. Braga, G. Blaise, J. Appl. Phys. 95 (2004) 2619.
[25] J. Cazaux, J. Appl. Phys. 59 (1986) 1418.
[26] R. Coelho, B. Aladeniz, B. Garros, D. Acroute, P. Mirebeau, IEEE Trans. Dielectr. Electr. Insul. 6 (1999) 202.
[27] R. Renoud, F. Mady, J.-P. Ganachaud, J. Phys.: Condens. Matter 14 (2002) 231.
[28] K. Kanaya, S. Okayama, J. Phys. D 5 (1972) 43.
[29] J.L. Giocondi, G.S. Rohrer, Chem. Mater. 13 (2001) 241.
[30] J.L. Giocondi, G.S. Rohrer, J. Am. Ceram. Soc. 86 (2003) 1182.
[31] J.L. Giocondi, G.S. Rohrer, J. Phys. Chem. B 105 (2001) 8275.
[32] X. Lei, D. Li, R. Shao, D.A. Bonnell, J. Mater. Res. 20 (2005) 712.
[33] Z. Hu, X. Lei, D.A. Bonnell (unpublished).